Optics and Spectroscopy, 2024, Vol. 132, No. 8

02

Oscillatory motion of Tamm polaritons in a magnetic field

© E.S. Sedov[1,2], M.M. Glazov[3], A.V. Kavokin[1,4]

[1] SOLAB Spin-optic laboratory, Saint-Petersburg state university, St. Petersburg, Russia
[2] Vladimir State University, Vladimir, Russia
[3] Ioffe Institute, St. Petersburg, Russia
[4] Abrikosov Center for Theoretical Physics, Moscow Institute of Physics and Technology, Dolgoprudnyi, Russia

E-mail: evgeny_sedov@mail.ru

Received May 16, 2024
Revised May 16, 2024
Accepted July 29, 2024

The oscillatory motion effect (Zitterbewegung) of Tamm polaritonic states at the interface of two multilayer binary heterostructures with overlapping band gaps, belonging to the C_{3v} point symmetry group and supporting excitonic resonance, has been theoretically investigated. The effect involves oscillations the trajectory of the Tamm state as it propagates along the interface plane. The possibility of controlling the characteristics of the oscillatory motion, including the period and amplitude of oscillations, through the use of an external magnetic field applied in the Faraday configuration, has been demonstrated.

Keywords: Tamm states, oscillatory motion, Zitterbewegung, exciton-polaritons, spin-orbit interaction.

DOI: 10.61011/EOS.2024.08.60024.6690-24

Introduction

Spatial dispersion effects in natural and artificial crystals, special role of which in the interaction processes between light and a substance was emphasized by V.M. Agranovich [1], are visualized very vividly for exciton polaritons in quantum microcavities [2]. This study is devoted to the theory of so-called Tamm exciton-polariton states that have been recently proposed by us in [3]. These are localized electromagnetic field states that occur at the interface of two optical heterostructures with different energy spectra in conditions of strong interaction between an electromagnetic field and environment disturbances. Surface states associated with the disturbance of one-electron potential periodicity near the crystal boundary were predicted by I.E. Tamm [4] in the simplest Kronig-Penney model. Similar surface or edge states are still extensively studied. Tamm states have been previously predicted for electrons at the semiconductor superlattice boundary [5] and also for optical modes at the interface of two multilayer binary dielectric heterostructures [6,7]. Both optical substructures can be formed from different [6] as well as from the same pairs of materials [7]. In the latter case, different thicknesses of layers of the same material in different substructures are chosen to ensure the difference in their energy spectra. Tamm states are formed in band gaps of both substructures to provide a prerequisite for them to occur — overlapping of these band gaps. In case of substructures formed from the same pairs of materials, this prerequisite is added by an evident requirement for these band gaps to have different sequence numbers.

Tamm states are also inherent in exciton-polariton systems. A photonic Tamm structure is transformed into a polaritonic structure when there is exciton resonance in the structure and strong coupling is ensured between the exciton and photon states with formation of mixed exciton-polariton modes. Exciton resonances occur when narrow quantum wells are integrated into the layers of one material in each substructure [8–10] or when a resonant material is used for layers of the same type [3,11].

Splitting of eigen s-modes (TE) and p-polarized modes (TM) is a typical feature of optical structures [12]. As a result, a doublet of Tamm polariton states with orthogonal polarizations is formed in a polaritonic structure near the exciton resonance [3]. An important advantage of polaritonic systems over photonic ones is the possibility to control their properties effectively, including dispersion and polarization properties, using an external impact.

Splitting of eigen states of the structure, besides the spectral splatter, leads to occurrence of new effects during quasiparticle propagation. One of the most prominent phenomena of this kind is an oscillatory motion (zitterbewegung). The effect is in spatial oscillations of the path of a free propagating particle. This effect was discussed at the dawn of the relativistic quantum theory [13,14] for free electrons, however, the most vivid manifestations of the effect are expected exactly in condensed media. This is due to a considerable decrease in the jitter frequency that is defined by the band gap $E_g/\hbar$ by order of magnitude (in units of reduced Planck's constant), rather than by the rest energy of a free electron $2m_0c^2/\hbar$ [15]. Besides semiconductors [15], the oscillatory motion phenomena was predicted and observed in several physical systems, including Bose–Einstein condensates of ultracold atoms [16], wave lattices [17] and graphene [18]. Zitterbewegung of photons and exciton polaritons is also known in semiconductor microcavities [19–23]. Display of the oscillatory motion of an electron induced by its spin precession is highly interesting [24]. The effect results from a spin-orbit interaction (real or artificial, associated with longitudinal and transverse splitting in case of polaritons) that involves mutual influence of the internal spin motion and external propagation of a particle in a structure (for the Tamm polariton states — in plane of the interface of the multilayer optical heterostructures).

We have shown in [3] that the Tamm polariton states can be excited at the interface of two binary layered resonance substructures. Occurrence of nonreciprocity in the propagation of such polaritons and removal of energy degeneracy between states corresponding to directions opposite to propagation in the structure plane when an external magnetic field is applied in the Faraday geometry have been also demonstrated. However, in [3], we were restricted to the discussion of Tamm state propagation in the structure plane in one direction (y axis) where degeneracy was removed. Physical limit corresponding to this case involves an endless wave packet width in the orthogonal direction x in the structure plane. Due to such conditions, we could identify the spin-orbit interaction effect on spin (polarization) properties of Tamm polariton states. This study focuses on the properties of Tamm states associated with propagation behavior in the structure plane. Using the generalized 4×4transfer matrix formalism, oscillatory motion of finite-width Tamm polariton wave packets has been studied theoretically. The effect of dispersion nonreciprocity on specific display of polariton zitterbewegung has been demonstrated. Possible control of zitterbewegung properties, in particular, oscillation period and amplitude, using an external magnetic field has been also demonstrated.

Studied structure

A structure proposed in [3] is examined (Figure 1, a). The structure consists of two multilayer substructures formed from 14 (top substructure) and 7 (bottom substructure) pairs of SiO_2/CdTe layers. The bottom substructure is placed on a SiO_2 substrate. The SiO_2 layers are taken as optically isotropic with the permittivity $\varepsilon_a = 2.25$. The CdTe layers serve as a resonant (bulk) medium with the exciton resonance energy $\hbar\omega_X \approx 1.67\,\mathrm{eV}$. The material is cubic semiconductor with the point symmetry group T_d. When the z axis is oriented along the [111] crystal axis, the structure is assigned to the point group C_{3v} (Figure 1, b). When there is an external magnetic field oriented along the $z \parallel [111]$, $\mathbf{B} = (0, 0, B)$ axis, permittivity tensor components of CdTe, $\hat{\varepsilon}_b = \hat{\varepsilon}_{b0} + \hat{\varepsilon}_{b1}(B) + \hat{\varepsilon}_{b2}(B, \mathbf{k})$ ($\mathbf{k}$ is the quasi-wave exciton vector), are written as:

$$\hat{\varepsilon}_{b0} = \bar{\varepsilon}_{b0}\left(1 + \frac{\omega_{LT}}{\omega_X - \omega - i\Gamma}\right)\hat{I}_3,$$

$$\hat{\varepsilon}_{b1}(B) = \begin{pmatrix} 0 & i\gamma_1 B & 0 \\ -i\gamma_1 B & 0 & 0 \\ 0 & 0 & 0 \end{pmatrix},$$

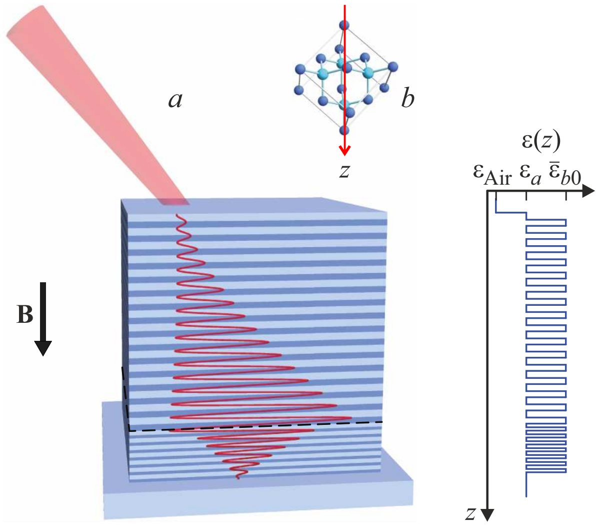

Figure 1. (a) Schematic diagram of the structure and optical excitation of the Tamm polariton state in the presence of external magnetic field applied in the structure growth direction. (b) CdTe lattice cell oriented in the coordinate axes of the studied structure. (c) Schematic diagram of the permittivity profile along the structure growth axis.

$$\hat{\varepsilon}_{b2}(B, \mathbf{k}) = \begin{pmatrix} -gBk_x & gBk_y & hBk_y \\ gBk_y & gBk_x & -hBk_x \\ hBk_y & -hBk_x & 0 \end{pmatrix},$$

where $\bar{\varepsilon}_{b0}$ is the background permittivity, ω_{LT} is the longitudinal-transverse exciton splitting frequency, Γ is the nonradiative exciton decay. Coefficient γ_1 characterizes the Zeeman splitting, g and h characterize the magneto-spatial dispersion [25–28]. It is the permittivity terms linear in $\mathbf{k}$ and $\mathbf{B}$ that are responsible for the asymmetric dispersion and nonreciprocal propagation of exciton polaritons in the system addressed in this work. The calculations use the following parameter values: $\bar{\varepsilon}_{b0} = 7.8$, $\hbar\omega_{LT} = 0.14\,\mathrm{meV}$, $\hbar\Gamma = 0.1\,\mathrm{meV}$, $\gamma_1 = 0.0002T^{-1}$, $g = -0.0008\,\mu\mathrm{m}/T$, $h = 0.004\,\mu\mathrm{m}/T$.

According to [3], selection of layer thicknesses is justified as follows. The bottom (belonging to the substrate) substructure is a distributed Bragg reflector for which the first-order Bragg resonance condition is met: $d_a^{\mathrm{bot}}\sqrt{\varepsilon_a} = d_b^{\mathrm{bot}}\sqrt{\varepsilon_{b0}} = \pi c/2\omega_{\mathrm{Br}}$, where c is the speed of light in vacuum, $d_{a,b}^{\mathrm{bot}}$ are the corresponding layer thicknesses of the bottom structure. The Bragg frequency ω_{Br} is selected such that the exciton resonance frequency ω_X coincides with the first photonic band gap of the mirror.

The top substructure is multi-layered, however, the Bragg resonance condition for it is violated in accordance with the following expression: $(d_a^{\mathrm{top}} + \delta d)\sqrt{\varepsilon_a} = (d_b^{\mathrm{top}} - \delta d)\sqrt{\varepsilon_{b0}} = \pi c/\omega_{\mathrm{Br}}$. As a result of the violation involving layer thickness variation by $\pm\delta d$, the second photonic band gap is opened. Moreover, as long as the layer thickness is approximately twice as large as the top substructure layer thicknesses, the first and second band gaps of the top and bottom substructures, respectively, are overlapped [3]. The calculations use the following parameter values: $d_a^{\rm bot} = 101.8$ nm, $d_b^{\rm bot} = 54.5$ nm, $d_a^{\rm top} = 148.6$ nm, $d_b^{\rm top} = 164.1$ nm, $\delta d = 55$ nm. Permittivity profile of the whole structure is shown schematically in Figure 1, *c*.

Calculation method

To study the dispersion properties of the structure and to simulate light propagation through the structure, we use the generalized 4×4 transfer matrix formalism that explicitly accounts for electromagnetic field polarization [29–33]. Using this approach, a system of Maxwell's equations is solved for each layer in the structure formed by multiple flat uniform layers, and the solutions agree at the neighboring layer boundaries.

Propagation of a light beam falling on the structure from the top substructure is addressed herein. The employed formalism is aimed at the analysis of propagation of plane monochromatic waves. Therefore, for the finite-width incident beam, the Fourier transformation in the microcavity plane shall be performed. This allows switching to a reciprocal space and then applying the transfer matrix formalism to each Fourier spectrum component [33].

When a plane wave with the frequency ω_0 propagates through the structure, tangential components of its wave vector, $\mathbf{k} = (k_x, k_y)$, are maintained when crossing a layer boundary. The normal component, k_z, varies in accordance with the dispersion properties of a particular layer. This variation ensures continuity of electric and magnetic fields and their derivatives at the layer boundary. The system of Maxwell's equations for a plane wave in layer j can be reduced to an eigen problem, $\kappa_j = k_{z,j}c/\omega_0$, of the characteristic matric $\hat{\Delta}_j$ for this layer:

$$\kappa_j \mathbf{\Psi}_j = \frac{c}{\omega_0}\hat{\Delta}_j \mathbf{\Psi}_j, \tag{1}$$

where $\mathbf{\Psi}_j = (E_{x,j}, H_{y,j}, E_{y,j}, H_{x,j})^T$ is the vector of the$x$- and y-components of the electric and magnetic fields. The characteristic matrix is generally set as follows:

$$\hat{\Delta}_j = \frac{1}{\varepsilon_{zz}} \times \begin{pmatrix} k_x\varepsilon_{zx} & k_x^2 - \varepsilon_{zz} & k_x\varepsilon_{zy} & -k_xk_y \\ \varepsilon_{xz}\varepsilon_{zx} - \varepsilon_{xx}\varepsilon_{zz} & k_x\varepsilon_{xz} & \varepsilon_{xz}\varepsilon_{zy} - \varepsilon_{xy}\varepsilon_{zz} & -k_y\varepsilon_{xz} \\ 0 & 0 & 0 & 1 \\ \varepsilon_{yx}\varepsilon_{zz} - \varepsilon_{yz}\varepsilon_{zx} + k_xk_y\varepsilon_{zz} & -k_x\varepsilon_{yz} & \varepsilon_{yy}\varepsilon_{zz} - \varepsilon_{yz}\varepsilon_{zy} - k_x^2\varepsilon_{zz} & -k_y\varepsilon_{yz} \end{pmatrix},$$

where $\varepsilon_{mm'}$ are the dielectric tensor components in layer j; $m, m' = x, y, z$. Derivation of the characteristic matrix $\hat{\Delta}_j$ and equation (1) is described in detail in [3,32–34].

Eigenvalues κ_j^l $[l = 1, \ldots, 4]$ in (1) correspond to effective wave vectors of waves with different polarizations ($\kappa_j^{1,3}$and and $\kappa_j^{2,4}$) propagating in layer j in the positive ($\kappa_j^{1,2}$) and negative ($\kappa_j^{3,4}$) directions of the z axes. Electric field in this basis is defined by the vector

$$\mathbf{E}_j = (E_j^1, E_j^2, E_j^3, E_j^4)^T. \tag{2}$$

In this case, coupling of the adjacent layers, $j-1$ and j, may be described as follows:

$$\mathbf{E}_{j-1} = \hat{A}_{j-1}^{-1}\hat{A}_j\hat{P}_j\mathbf{E}_j. \tag{3}$$

In (3), the interaction matrix $\hat{A}_j$ is used to project the vector $\mathbf{E}_j$ on the vector $\mathbf{\Psi}_j$. $\hat{A}_j$ is built such that its columns form eigen vectors of the characteristic matrix $\hat{\Delta}_j$ derived from solution of equation (1). Basically, field propagation through layer j (from the front edge of the layer, z_j, to the rear edge, $z_j + d_j$, where d_j is the layer thickness) is described by the propagation matrix $\hat{P}_j$ whose components are defined as $\hat{P}_j^{ll'} = \delta_{ll'} \exp[i(\omega_0/c)\kappa_j^l d_j]$, where $\delta_{ll'}$ is the Kronecker symbol. Though the model includes terms that are linear in the wave vector $\mathbf{k}$ in the layer permittivity, the presence of only tangential electric field components in (2) avoids the need to introduce additional boundary conditions at layer interfaces. The inlet field vector, $\mathbf{E}_0$, is related to the outlet field vector, $\mathbf{E}_{N+1}$, of the structure consisting of N layers through the following equation

$$\mathbf{E}_0 = \hat{T}\mathbf{E}_{N+1} = \hat{A}_0^{-1}(\Pi_{j=1}^N \hat{A}_j\hat{P}_j\hat{A}_j^{-1})\hat{A}_{N+1}, \tag{4}$$

where index $N+1$ is used to designate a continuous medium adjacent to layer N. $\hat{T}$ is a transfer matrix through the structure.

Note that, when there is no external magnetic field ($B = 0$), basis (2) is composed of the s- and p-polarized waves. However, the presence of magnetic field induces optical property anisotropy of the structure leading to polarization mixing. In this case, when describing radiation transmission through particular layers, it is correct to suggest ordinary and extraordinary wave propagation in them [35].

Tamm polariton state condition and dispersion

The main arguments providing the Tamm polariton condition are discussed in detail in [3,36]. For the sake of completeness, they are summarized briefly below. Imagine a plane of the interface of two substructures. Let's consider propagation of two oppositely directed randomly polarized waves from this plane deep into each of the substructures. Each of the waves undergoes reflection from the corresponding substructure that is characterized by the amplitude reflection coefficients$\hat{r}^L$, where $L = \text{top}$ and $L = \text{bot}$ for the top and bottom substructures, respectively. $\hat{r}^L$ are given by the 2×2 matrices whose diagonal elements, r_{pp}^L and r_{ss}^L, characterize wave reflection without polarization variation. The external magnetic field $\mathbf{B}$ induces polarization mixing, therefore the off-diagonal elements r_{ps}^L and r_{sp}^L that characterize wave reflection with polarization reversing are

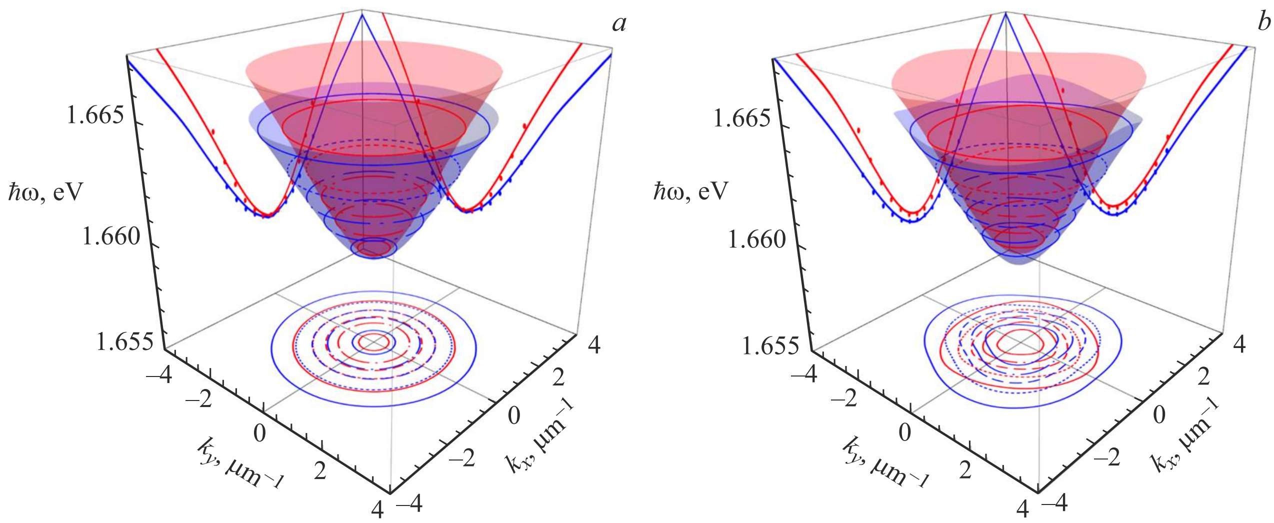

Figure 2. Dispersion of Tamm polariton states at $B = 0$ (a), 10 T (b) calculated by solving equations (5) within the generalized 4×4 transfer matrix formalism. The two-dimensional images were made at $k_x = 0$ (right), $k_y = 0$ (left). Dispersion curves plotted from Hamiltonian (6) are shown dotted. Equifrequency outlines (bottom) correspond to cross-sections in the three-dimensional image.

generally non-zero. To avoid overloading with additional symbols, we use s and p for waves both in optically isotropic and anisotropic layers. For the Tamm polariton state to exist, a field of a specified polarization at the interface being part of one of the substructures (top or bottom) must coincide with the field of the same polarization that is reflected from the other substructure (bottom or top, respectively). Taking into account polarization mixing, the Tamm polariton state condition is written as [3]:

$$(r_{ss}^{\mathrm{top}} r_{ss}^{\mathrm{bot}} + r_{ps}^{\mathrm{top}} r_{sp}^{\mathrm{bot}}) \cos\theta + (r_{pp}^{\mathrm{top}} r_{pp}^{\mathrm{bot}} + r_{sp}^{\mathrm{top}} r_{ps}^{\mathrm{bot}} - 1) \sin\theta = 0, \tag{5a}$$

$$(r_{pp}^{\mathrm{top}} r_{pp}^{\mathrm{bot}} + r_{sp}^{\mathrm{top}} r_{ps}^{\mathrm{bot}} - 1) \cos\theta + (r_{ss}^{\mathrm{top}} r_{ss}^{\mathrm{bot}} + r_{ps}^{\mathrm{top}} r_{sp}^{\mathrm{bot}}) \sin\theta = 0, \tag{5b}$$

where θ is the complex parameter characterizing the Tamm state polarization. Reflection coefficients may be calculated in accordance with the following expressions:

$$r_{(pp,ss)} = [T_{(31,42)} T_{(22,11)} - T_{(32,41)} T_{(21,12)}]/\det\hat{T}$$

and

$$r_{(ps,sp)} = [T_{(41,32)} T_{(22,11)} - T_{(42,31)} T_{(21,12)}]/\det\hat{T}.$$

When there is no external magnetic field ($B = 0$), conditions (5) for the polarizations s and p are separated and reduced to a simplified form: $r_{nn}^{\mathrm{top}} r_{nn}^{\mathrm{bot}} = 1$, $n = s, p$ [36].

By solving equations (5) within the generalized 4×4 transfer matrix formalism, dispersion of the Tamm polariton state doublet in the structure plane can be calculated. Figure 2 shows dispersion surfaces obtained by magnetic field induction $B = 0$ and 10 T. When no external magnetic field is applied (Figure 2, a), the dispersion of eigen (s- and p-polarized) modes has axial symmetry. When an external magnetic field is applied (Figure 2, b), the dispersion has only a third-order axis of rotation, $C_3 \parallel z$, there is also a mirror reflection$x \to -x$ [3].

Tamm polariton state zitterbewegung

Let's consider transition of a continuous laser beam through the described structure within the generalized transfer matrix formalism. Select a Gaussian-shaped beam:

$$\mathbf{E}_0 \propto \exp[-\mathbf{r}^2/2w^2 + i(k_0 y - \omega_0 t)]\mathbf{p}_0,$$

with the width w, where $\mathbf{r} = (x, y)$. ω_0 is the laser frequency. The beam falls on the structure at an angle in the yz plane, so that its wave vector in the structure plane $\mathbf{k}_0 = (0, k_0)$. The wave number k_0 is selected such that to be in the middle between the split dispersion branches in Figure. 2, b at the specified frequency ω_0. Thus, the superposition of eigen states may be excited most effectively. The vector column $\mathbf{p}_0$ characterizes the incident radiation polarization. Circular polarization is selected and is set as $\mathbf{p}_0 = (1, i, p_3, p_4)^T$ in basis (2) in all numerical experiments, where p_3 and p_4 are found from (4) in a self-consistent way.

Figure 3 shows the normalized intensity distribution $I(\mathbf{r}) = |E_x(\mathbf{r})|^2 + |E_y(\mathbf{r})|^2$and the Stokes vector component (polarization component) distribution:

$$S_x(\mathbf{r}) = \left(|E_x(\mathbf{r})|^2 - |E_y(\mathbf{r})|^2\right)/I(\mathbf{r}),$$

$$S_y(\mathbf{r}) = 2\mathrm{Re}[E_x(\mathbf{r})E_y^*(\mathbf{r})]/I(\mathbf{r}),$$

$$S_z(\mathbf{r}) = -2\mathrm{Im}[E_x(\mathbf{r})E_y^*(\mathbf{r})]/I(\mathbf{r}),$$

Tamm polariton states in plane of the substructure interface determined with $B = -5$ T and the wave numbers $k_0 = -1$ (a–d), 1 μm (e–h). $E_x(\mathbf{r})$ and $E_y(\mathbf{r})$ characterize the electric field distribution in the x and y polarizations in the corresponding plane. Center-of-mass paths of the wave packets, $X(y) = \int xI(\mathbf{r})dx / \int I(\mathbf{r})dx$, are shown by green curves above the intensity distributions in Figure 3, a, e.

The zitterbewegung takes place in both examined cases: intensity distribution is non-monotonic with pronounced oscillations in a direction transverse to the wave packet propagation direction. It is shown that the oscillation period is different in different cases and depends on the propagation direction.

Oscillations of the center-of-mass path of the Tamm polariton states are also accompanied by the oscillations of their degree of polarization with the same period (Figure 3, *b–d,f–h*). Interestingly, the polarization component S_x of the Tamm polariton state (Figure 3, *b,f*) also undergoes oscillations in the vicinity of the center line of the wave packet $x = 0$ as opposed to the polariton zitterbewegung in the planar zitterbewegung induced only by the TE−TM-splitting predicted in [20].

Figure 4 shows the intensity distribution of the described Tamm polariton states in the conjugate space, $I(\mathbf{k})$, compared with the spatial spectrum of the eigen Tamm polariton state doublet. It is shown that despite the same (with an accuracy to the wave vector sign) excitation conditions, the eigen states have different splitting which leads to a different oscillation period. This is the display of magnetically-induced nonreciprocity in the studied system.

Zitterbewegung control using an external magnetic field

It is convenient to consider the effects induced by the spin-orbit interaction within the pseudospin formalism [37]. The symmetry analysis performed previously in [3] makes it possible to write the effective Hamiltonian of the Tamm polariton state doublet in the basis of the right and left circular polarizations:

$$H = \frac{\hbar^2 k^2}{2M} + \hbar\mathbf{\Omega}\cdot\mathbf{s}, \tag{6}$$

where $\mathbf{k} = (k_x, k_y)$ is the polariton wave vector in the structure plane, M is effective mass of polariton, and $\propto \mathbf{\Omega}\cdot\mathbf{s}$ is responsible for the polarization mode splitting. Polariton polarization is associated with a pseudo-spin having two projections on the structure growth axis: $\mathbf{s} = \frac{1}{2}\boldsymbol{\sigma}$ is the polariton pseudo-spin operator, $\boldsymbol{\sigma} = (\sigma_x, \sigma_y, \sigma_z)$ is the Pauli matrix vector. unit operator of the first summand on the right-hand side (6) is omitted for clarity. Within the pseudospin formalism, it is convenient to characterize the dispersion branch splitting using the vector $\mathbf{\Omega} = (\Omega_x, \Omega_y, \Omega_z)$ that serves as an effective magnetic field inducing the polariton pseudospin precession. Components of $\mathbf{\Omega}$ for the Tamm state doublet are written as:

$$\Omega_x = C_2[(k_x^2 - k_y^2)] + C_3 B k_y, \tag{7a}$$

$$\Omega_y = 2k_x k_y C_2 + C_3 B k_x, \tag{7b}$$

$$\Omega_z = C_1 B. \tag{7c}$$

C_1 in (7c) characterizes the Zeeman splitting in circular polarizations in the external magnetic field $\mathbf{B} = (0, 0, B)$. C_2 describes the TE−TM-splitting of the Tamm polariton modes. Summands with C_3 characterize magneto-spatial dispersion that occurs in structures with point symmetry C_{3v} [3,38]. Eigenvalues of Hamiltonian (6) depending on k_x at $k_y = 0$ and on k_y at $k_x = 0$ are shown in the side panes in Figure 2, *a* and *b*, respectively, for $B = 0$ and 10 T compared with the Tamm polariton state doublet dispersions calculated within the generalized transfer matrix formalism. Splitting constants and effective polariton mass in the structure plane are estimated as $\hbar C_1 = 15\,\mu$eV/T, $\hbar C_2 = 0.54\,\text{meV}\cdot\mu\text{m}^2$, $\hbar C_3 = 30\,\mu\text{eV}\cdot\mu$m/T and $M = 3.4\cdot 10^{-5} m_0$, where m_0 is the free electron weight.

Equations for the Tamm polariton state doublet coordinate operators in the structure plane are derived as follows:

$$\partial_t x = \frac{\hbar k_x}{M} + 2C_2[k_x s_x + k_y s_y] + C_3 B s_y,$$

$$\partial_t y = \frac{\hbar k_y}{M} + 2C_2[k_x s_y - k_y s_x] + C_3 B s_x.$$

As can be seen, polariton pseudospin evolution described by the precession equation $\partial_t \mathbf{s} = \mathbf{\Omega}\times\mathbf{s}$contributes to the polariton path „jitter" compare with [24].

Consider the Tamm polariton state propagation along the substructure boundary characterized by spinor $|\Psi\rangle = \Psi(\mathbf{r})|\psi\rangle$, where

$$\Psi(\mathbf{r}) = (2\pi)^{-1}\int_{-\infty}^{\infty}\Psi(\mathbf{k}-\mathbf{k}_0)e^{i\mathbf{kr}}d\mathbf{k}$$

— is the wave function envelope, $|\psi\rangle$ describes the Tamm state polarization. Propagation of circularly polarized wave packet, $|\psi\rangle = (1, 0)$, along the y axis is an important case, $\mathbf{k}_0 = (0, k_0)$. In this case, for a considerably wide wave packet (for whose width condition $d \gg 2\pi/k_0$ is met), analytical expression for the center-of-mass path, $X(Y)$, may be derived where $X(t) = \langle\Psi|x|\Psi\rangle$ and $Y(t) = \langle\Psi|y|\Psi\rangle$:

$$X(t) = -\frac{\Omega'_{y0}\Omega_{x0}}{\Omega_0^2}(1 - \cos\Omega_0 t), \tag{8a}$$

$$Y(t) = \frac{\hbar}{M}k_0 t + \frac{\Omega_{x0}\Omega'_{x0}}{\Omega_0^2}C_1 B\left(t - \frac{1}{\Omega_0}\sin\Omega_0 t\right), \tag{8b}$$

where

$$\Omega_{x0} = \Omega_x|_{\mathbf{k}\to\mathbf{k}_0} = C_3 B k_0 - C_2 k_0^2,$$

$$\Omega'_{x0} = (\partial\Omega_x/\partial k_x)|_{\mathbf{k}\to\mathbf{k}_0} = BC_3 - 2C_2 k_0,$$

$$\Omega'_{y0} = (\partial\Omega_y/\partial k_x)|_{\mathbf{k}\to\mathbf{k}_0} = BC_3 + 2C_2 k_0$$

and

$$\Omega_0 = \sqrt{\Omega_{x0}^2 + \Omega_{y0}^2 + \Omega_{z0}^2}.$$

Pseudo spin vector component evolution $\mathbf{S}(t) = \langle\mathbf{s}\rangle$ in this case is described by the following expressions:

$$S_x(t) = \frac{BC_1\Omega_{x0}}{\Omega_0^2}(1 - \cos\Omega_0 t), \tag{9a}$$

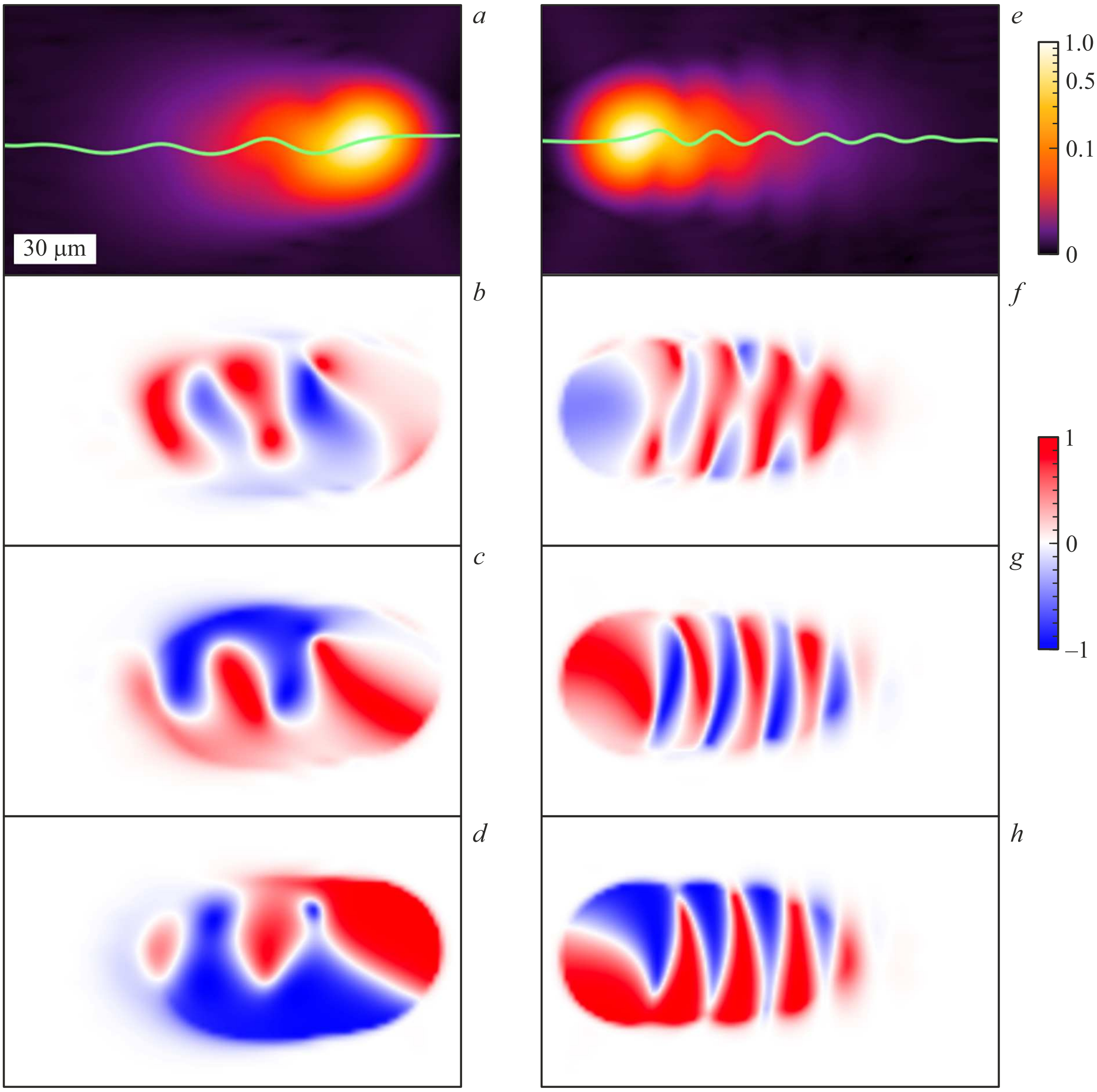

Figure 3. Oscillatory motion of the Tamm polariton states in an external magnetic field with induction $B = -5\,\mathrm{T}$ with excitation by the inclined Gaussian laser beam $7\,\mu$m in width with the energy$\hbar\omega_0 = 1.66035\,\mathrm{eV}$ and quasi-pulse $k_0 = -1$ $(a{-}d)$, $1\,\mu\mathrm{m}^{-1}$ $(e{-}h)$. Exciting radiation polarization is circular. Spatial distribution of intensity (a, e) and of the Stokes vector components S_x (b,f), S_y (c,g) and S_z (d,h) of the Tamm polariton states in the plane at the substructure interface calculated by the generalized 4×4 transfer matrix method are shown in the panes. Green curves in (a, e) show the center-of-mass path of the Tamm polariton state.

$$S_y(t) = -\frac{\Omega_{x0}}{\Omega_0}\sin\Omega_0 t, \tag{9b}$$

$$S_z(t) = \frac{B^2C_1^2 + \Omega_{x0}^2}{\Omega_0^2}\cos\Omega_0 t. \tag{9c}$$

Without an external magnetic field, $B = 0$, expressions (8) and (9) are considerably simplified and coincide with those derived for the polaritons in a planar microcavity [21]:

$$X(t) = -(2/k_0)(1-\cos\Omega_0 t),\quad Y(t) = \hbar k_0 t/M,$$

$$\mathbf{S}(t) = (0, -\sin\Omega_0 t, \cos\Omega_0 t).$$

It is shown that at $B = 0$ the Stokes parameter S_x that is responsible for the degree of linear polarization in the (xy) axes actually remains unchanged during the evolution of the Tamm polariton state. However, the presence of an external magnetic field induces its oscillations together with other components as shown in Figure 3, *b,f*.

Spatial oscillation period of the Tamm polariton state has a quadratic dependence both on the wave number k_0 and the external field induction B. This is supported by the dependences of the period on k_0 with fixed B, and on B with fixed k_0, as shown in Figure 5, *a, c*. The

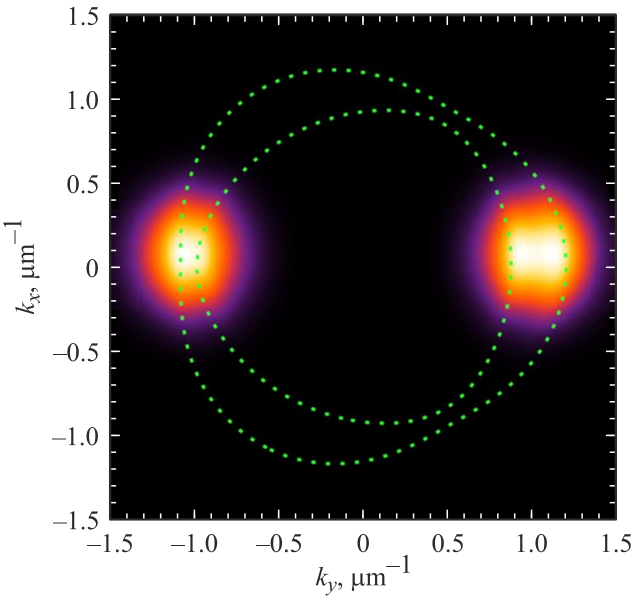

Figure 4. Intensity distribution of the Tamm states shown in Figure 3, a–d (left) and in Figure 3, e–h (right) in the conjugate space. Green dashed curves are the energy constant lines of the Tamm polariton states at $\hbar\omega = 1.66035$ eV and $B = -5$ T.

solid lines demonstrate dependences derived from analytical expressions (8). Dot indicate the results of simulation of propagation of the Tamm polariton states excited by the laser beam with the finite width $w = 7\,\mu$m within the generalized 4×4 transfer matrix formalism. It is shown that, in the range of values where numerical calculation appeared to be possible, the difference of the infinitely wide wave packet on the analytical limit without considering the dissipation is not higher than the numerical calculation error. The same result (not shown in the article) has been obtained for exciting beams of other width in the range from 5 to $50\,\mu$m. Finite computational grid size and pitch in the numerical experiment and , in some cases, fast (compared with the period) Tamm state decay with distance from the excitation point hinder the assessment o the spatial oscillation period in random wave number and magnetic induction ranges.

Dependence of amplitude on k_0 and B is more complex. With fixed B, dependence on k_0 has a pronounced peak (Figure 5, b). On the contrary, the dependence on B with fixed k_0 has a dip at $B = 0$. Note that analytical expressions (8) do not predict the zitterbewegung amplitudes in conditions close to experimental. We reproduce these amplitudes through numerical simulation within the generalized 4×4 transfer matrix formalism. This coincides with the conclusion applicable to the polariton zitterbewegung in the planar microcavity [21]. The reasons are as follows. First, analytical expressions (8) do not account for oscillation decay that takes place for the finite-width wave packets (Figure 3, a, e). The wider the wave packet spectrum the shorter, of course, the decay length. Therefore, the amplitude in Figure 5, b, d implies the maximum deviation of the path of the Tamm polariton state nearest to the point of laser beam entry into the structure. Second, the presence of continuous optical pumping affects the path deviation. This becomes more vivid, the closer pumping spot size gets to the oscillation period. Finally, the Tamm polariton state decay makes its contribution with distance from the pumping spot. Detailed analysis of these factors is not in the scope of this work.

Conclusion

This study describes theoretically the oscillatory motion (zitterbewegung) of the Tamm polariton states in the resonant optical structure formed from two multilayer SiO_2/CdTe substructures. The effect is in oscillations of the Tamm state path propagating in the substructure interface plane. The effect occurs for the finite-width Tamm polariton wave packets and results from the impact of the Tamm polariton pseudospin (polarization) on polariton propagation in the spin-orbit interaction conditions caused by polarization mode splitting, including the TE–TM-splitting and magnetically-induced splitting. Path oscillations are followed by polarization oscillations predicted by us previously for the case of one-dimensional propagation of the Tamm polaritons in the structure plane [3].

Magnetic field applied in the Faraday geometry modifies the polarization and dispersion characteristics of the Tamm polaritons, in particular, leads to dispersion nonreciprocity. This implies variation of the strength and manner of eigen mode splitting in the structure and, consequently, variation of the contribution made by the spin-orbit interaction to the Tamm polariton state propagation. The study shows the external magnetic field effect on the oscillatory motion properties and intensities and demonstrates controllability of the Tamm polariton path oscillation period and amplitude using an external magnetic field.

Funding

E.S.S and A.V.K. are grateful to St.Petersburg State University (Grant № 122040800257-5). The work was performed by E.S.S. under the state assignment for research of the Ministry of Science and Higher Education of the Russian Federation (topic FZUN-2024-0019, state assignment of Vladimir State University). A.V.K. is grateful to Moscow Institute of Physics and Technology under the „Proritet-2030" Strategic Academic Leadership Program. Symmetry analysis and analytical models were developed under the sponsorship of the Russian Science Foundation, Grant № 23-12-00142 (M.M.G.).

Conflict of interest

The authors declare that they have no conflict of interest.

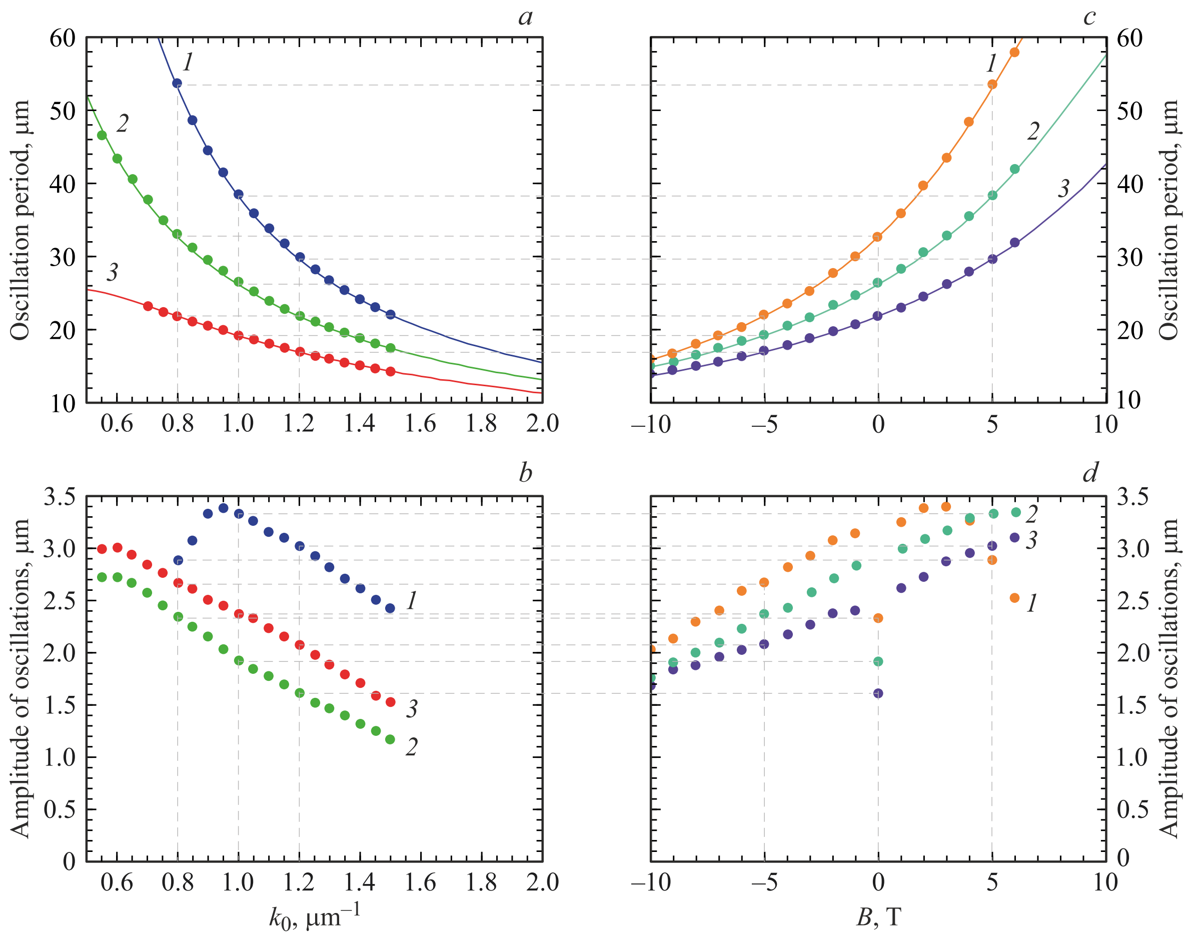

Figure 5. Dependence of the oscillation period (a, c) and amplitude (b, d) of the Tamm polariton state path: a, b — on the wave number in the structure plane k_0 with fixed external magnetic field inductions; c, d — on the external magnetic field induction B with fixed wave numbers. In panes (a, b) $B = 5$ (*1*), 0 (*2*), -5 T (*3*). In panes (c, d) $k_0 = 0.8$ (*1*), 1 (*2*), 1.2 μm^{-1} (*3*). Solid curves in panes (*a*) and (*c*) indicate dependences obtained from analytical expressions (8); color dots show the numerical calculation results within the generalized 4×4 transfer matrix formalism; dashed lines connect dots with the same k_0 and B.

References

[1] V.M. Agranovich, V.L. Ginzburg. *Kristallooptika s uchetom prostranstvennoy dispersii i teoriya eksitonov* (Nauka, M., 1965) (in Russian).

[2] A. Kavokin, J.J. Baumberg, G. Malpuech, F.P. Laussy. *Microcavities* (Oxford University Press, Oxford, UK, 2011).

[3] E. Sedov, M. Glazov, A. Kavokin. Phys. Rev. Appl., **17** (2), 024037 (2022). DOI: 10.1103/PhysRevApplied.17.024037

[4] I.E. Tamm. ZhETF, **3**, 34 (1933). (in Russian).

[5] M.R. Vladimirova, A.V. Kavokin. Phys. Solid State, **37** (7), 1178 (1995).

[6] H.Y. Dong, J. Wang, K.H. Fung. Opt. Lett., **38** (24), 5232 (2013). DOI: 10.1364/OL.38.005232

[7] A.V. Kavokin, I.A. Shelykh, G. Malpuech. Phys. Rev. B, **72** (23), 233102 (2005). DOI: 10.1103/PhysRevB.72.233102

[8] A. Askitopoulos, L. Mouchliadis, I. Iorsh, G. Christmann, J.J. Baumberg, M.A. Kaliteevski, Z. Hatzopoulos, P.G. Savvidis. Phys. Rev. Lett., **106** (7), 076401 (2011). DOI: 10.1103/PhysRevLett.106.076401

[9] E.S. Sedov, I.V. Iorsh, S.M. Arakelian, A.P. Alodjants, A. Kavokin. Phys. Rev. Lett., **114** (23), 237402 (2015). DOI: 10.1103/PhysRevLett.114.237402

[10] E.S. Sedov, E.D. Cherotchenko, S.M. Arakelian, A.V. Kavokin. Phys. Rev. B, **94** (12), 125309 (2016). DOI: 10.1103/PhysRevB.94.125309

[11] F. Biancalana, L. Mouchliadis, C. Creatore, S. Osborne, W. Langbein. Phys. Rev. B, **80** (12), 121306 (2009). DOI: 10.1103/PhysRevB.80.121306

[12] G. Panzarini, L.C. Andreani, A. Armitage, D. Baxter, M.S. Skolnick, V.N. Astratov, J.S. Roberts, A.V. Kavokin, M.R. Vladimirova, M.A. Kaliteevski. Phys. Rev. B, **59** (7), 5082 (1999). DOI: 10.1103/PhysRevB.59.5082

[13] G. Breit. Proc. National Academy of Sciences, **14**, 553 (1928). DOI: 10.1073/pnas.14.7.553

[14] E. Schrödinger. Berliner Ber., P. 418–428 (1930).

[15] W. Zawadzki. Phys. Rev. B, **72** (8), 085217 (2005). DOI: 10.1103/PhysRevB.72.085217

[16] M. Merkl, F.E. Zimmer, G. Juzeli¯unas, P. Öhberg. Europhys. Lett., **83** (5), 54002 (2008). DOI: 10.1209/0295-5075/83/54002

[17] F. Dreisow, M. Heinrich, R. Keil, A. Tünnermann, S. Nolte, S. Longhi, A. Szameit. Phys. Rev. Lett., **105** (14), 143902 (2010). DOI: 10.1103/PhysRevLett.105.143902

[18] T.M. Rusin, W. Zawadzki. Phys. Rev. B, **76** (19), 195439 (2007). DOI: 10.1103/PhysRevB.76.195439
[19] E. Sedov, I. Sedova, S. Arakelian, A. Kavokin. Opt. Lett., **46** (8), 1836–1839 (2021). DOI: 10.1364/OL.418337
[20] E.S. Sedov, Y.G. Rubo, A.V. Kavokin. Phys. Rev. B, **97** (24), 245312 (2018). DOI: 10.1103/PhysRevB.97.245312
[21] E.S. Sedov, I.E. Sedova, S.M. Arakelian, A.V. Kavokin. New J. Phys., **22** (8), 083059 (2020). DOI: 10.1088/1367-2630/aba731
[22] I.E. Sedova, E.S. Sedov, S.M. Arakelian, A.V. Kavokin. Bull. Russ. Acad. Sci.: Physics, **84** (12), 1453–1458 (2020). DOI: 10.3103/S1062873820120333.
[23] S. Lovett, P.M. Walker, A. Osipov, A. Yulin, P.U. Naik, C.E. Whittaker, I.A. Shelykh, M.S. Skolnick, D.N. Krizhanovskii. Light. Sci. Appl., **12**, 126 (2023). DOI: 10.1038/s41377-023-01162-x
[24] S.A. Tarasenko, A.V. Poshakinskiy, E.L. Ivchenko, I. Stepanov, M. Ersfeld, M. Lepsa, B. Beschoten. JETP Lett., **108** (5), 326–328 (2018). DOI: 10.1134/S0021364018170022.
[25] O.V. Gogolin, V.A. Tsvetkov, E.G. Tsitsishvili. JETP, **60** (3), 593 (1984).
[26] B.B. Krichevtsov, R.V. Pisarev, A.A. Rzhevskiĭ, H.-J. Weber. JETP Lett., **69** (7), 551 (1999).
[27] T. Godde, M.M. Glazov, I.A. Akimov, D.R. Yakovlev, H. Mariette, M. Bayer. Phys. Rev. B, **88** (15), 155203 (2013). DOI: 10.1103/PhysRevB.88.155203
[28] L.V. Kotova, V.N. Kats, A.V. Platonov, V.P. Kochereshko, R. André, L.E. Golub. Phys. Rev. B, **97** (12), 125302 (2018). DOI: 10.1103/PhysRevB.97.125302
[29] P. Yeh. J. Opt. Soc. Am., **69** (5), 742 (1979). DOI: 10.1364/JOSA.69.000742
[30] D.W. Berreman. J. Opt. Soc. Am., **62** (4), 502 (1972). DOI: 10.1364/JOSA.62.000502
[31] W. Xu, L.T. Wood, T.D. Golding. Phys. Rev. B, **61** (3), 1740 (2000). DOI: 10.1103/PhysRevB.61.1740
[32] N.C. Passler, A. Paarmann. J. Opt. Soc. Am. B, **34** (10), 2128 (2017). DOI: 10.1364/JOSAB.34.002128
[33] G.D. Landry, T.A. Maldonado. Appl. Opt., **35** (30), 5870 (1996). DOI: 10.1364/AO.35.005870
[34] E.S. Sedov, M.M. Glazov, P.G. Lagoudakis, A.V. Kavokin. Phys. Rev. Research, **6** (2), 023220 (2024). DOI: 10.1103/PhysRevResearch.6.023220
[35] N.C. Passler, M. Jeannin, A. Paarmann. Phys. Rev. B, **101** (16), 165425 (2020). DOI: 10.1103/PhysRevB.101.165425
[36] M. Kaliteevski, I. Iorsh, S. Brand, R.A. Abram, J.M. Chamberlain, A.V. Kavokin, I.A. Shelykh. Phys. Rev. B, **76** (16), 165415 (2007). DOI: 10.1103/PhysRevB.76.165415
[37] K.V. Kavokin, I.A. Shelykh, A.V. Kavokin, G. Malpuech, P. Bigenwald. Phys. Rev. Lett., **92** (1), 017401 (2004). DOI: 10.1103/PhysRevLett.92.017401
[38] M.M. Glazov, F. Dirnberger, V.M. Menon, T. Taniguchi, K. Watanabe, D. Bougeard, J.D. Ziegler, A. Chernikov. Phys. Rev. B, **106** (12), 125303 (2022). DOI: 10.1103/PhysRevB.106.125303

Translated by E.Ilinskaya